

---

This manuscript is prepared for *The Journal of Physical Chemistry C*. Please note that, the manuscript is a non-peer reviewed preprint submitted to EarthArXiv. The final printed version of this manuscript may have slightly different content and will be available via the 'Peer-reviewed Publication DOI' link. Please feel free to contact the corresponding author. Any feedback will be greatly appreciated.

---

1 **Energetics of Interfacial Interactions of Hydrocarbon Fluids with Kerogen and**  
2 **Calcite using Molecular Modeling**

3

4 Zelong Zhang,<sup>\*,†</sup> Haoran Liu,<sup>‡,⊥</sup> and Jianwei Wang<sup>†,§</sup>

5

6 <sup>†</sup>Department of Geology and Geophysics, Louisiana State University, Baton Rouge, LA  
7 70803, United States

8 <sup>‡</sup>Department of Experimental Statistics, Louisiana State University, Baton Rouge, LA  
9 70803, United States

10 <sup>⊥</sup>Department of Oceanography and Coastal Sciences, Louisiana State University, Baton  
11 Rouge, LA 70803, United States

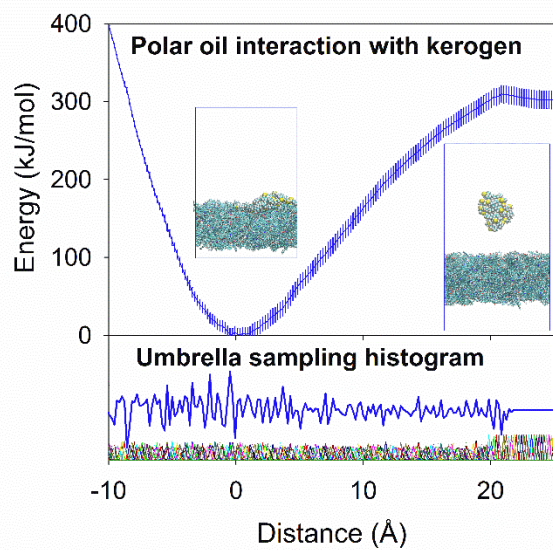
12 <sup>§</sup>Center for Computation and Technology, Louisiana State University, Baton Rouge, LA  
13 70803, United States

14 Corresponding to: zelongz@lsu.edu

15

16 **Abstract**

17 Understanding the fluid-rock interactions is essential to characterize the behavior of petroleum  
18 fluids in reservoir formations. Such understanding is difficult to obtain due to the heterogeneous  
19 nature of hydrocarbon systems. This study investigated the interactions of light oil molecules  
20 with kerogen and calcite using Molecular Dynamics simulations. Specifically, octane and  
21 octanthiol were used as model molecules for non-polar and polar oil compounds; a kerogen  
22 fragment molecule was employed as the building block for kerogen, the major constituent of  
23 reservoir rock organics; calcite as a model system for hydrophilic materials in reservoir rocks.  
24 Umbrella Sampling method combined with the Weighted Histogram Analysis Method was  
25 deployed to calculate the free energy profiles of oil molecule desorption from kerogen and  
26 calcite surfaces. The effects of oil molecular polarity, size of oil molecular cluster, and the  
27 presence of water on the interfacial interactions were evaluated based on the free energy profile  
28 of desorption. The results show the free energy of desorption of oil molecules significantly  
29 decreases at both kerogen and calcite surfaces if water is presented. For the polar oil molecule,  
30 the free energy of desorption is higher than that of non-polar oil at both calcite and kerogen  
31 surfaces. The kerogen surface exhibits stronger binding energies of oil molecules than the  
32 calcite. These findings suggest that 1) polar oil compounds require more effort to be recovered  
33 than non-polar ones from the reservoir rocks, 2) isolated oil molecules or oil clusters of a smaller  
34 size are harder to be displaced from the surfaces than a larger size of molecular clusters, and 3)  
35 the presence of water decreases the free energy of desorption at both surfaces. The results  
36 provide an energetic perspective of the interfacial interactions for the oil recovery in reservoir  
37 formations. This study demonstrates that the capability of MD simulation in evaluating the  
38 impact of different factors on the interfacial interactions for the fundamental understanding of  
39 the oil recovery processes in petroleum reservoirs, which can provide valuable implications for  
40 developing novel technologies of oil recovery.



43 **1 Introduction**

44 Oil is the main energy source for our modern civilization and will remain as a major  
45 contributor of global energy in the foreseeable future.<sup>1</sup> However, only a portion of oil preserved  
46 in a reservoir can be recovered. Thus, it is imperative to improve the recovery efficiency of  
47 petroleum reservoirs. Current methods to improve oil production including primary, secondary,  
48 and tertiary oil recovery techniques can yield 30 to 60 % of the original oil in place, leaving up to  
49 70% of the original oil in a reservoir.<sup>1,2</sup>

50 The pressing demand of energy from modern civilization has spurred technical  
51 innovations to improve oil recovery, especially through tertiary oil recovery or enhanced oil  
52 recovery. However, there is a limited understanding of how hydrocarbon-bearing fluids interact  
53 with the materials in reservoir formations. This knowledge gap impairs the assessment of the  
54 economic potential of a hydrocarbon reservoir. For example, relative permeability, an essential  
55 parameter of fluid flow characteristics for formation evaluation, is measured by Special Core  
56 Analysis (SCAL) through conducting flow experiments on core plugs taken from a reservoir.  
57 However, SCAL results are often contradictory or cannot be properly implemented in the  
58 reservoir modelling and petrophysical evaluation.<sup>3-5</sup> A myriad of factors may complicate the  
59 results, including the hydrofracture geometries, networks of preexisting fractures, adsorption and  
60 desorption processes, non-Darcy multiphase flow, chemically and structurally heterogeneous  
61 formations, etc.<sup>6</sup>

62 The interfacial interactions between the fluid and rock play a key role in all these  
63 complications. As shown in Figure 1, if a pore has a less than 100 nm radius and the  
64 intermolecular interaction has an effective distance of 3 nm, a significant portion (12% – 100%  
65 volume) of confined fluid can be directly affected by the interfacial interactions. Therefore, to

66 further improve recovery efficiency, a fundamental understanding of the fluid-rock interactions  
67 is indispensable.

68 To probe the interfacial interactions at nanoscales, molecular-level characterization is  
69 necessary. Both experimental and computational approaches have been applied to study the  
70 hydrocarbon fluid behavior in the rock at nanoscale. Extensive experimental studies have been  
71 conducted on the reservoir formations to characterize the organic content<sup>7,8</sup>, pore structure<sup>9-12</sup>,  
72 and petrophysical properties<sup>11,13-15</sup>. These studies aimed to calibrate the empirical models in  
73 reservoir engineering to describe the fluid flow<sup>16,17</sup> and to provide a basis for reservoir  
74 assessment and production optimization.<sup>18</sup> However, due to the compositional and structural  
75 heterogeneity of reservoir formations, it is challenging to interpret the dynamics and kinetics of  
76 interface interactions without knowing the molecular scale details. Current understanding of the  
77 hydrocarbon systems heavily relies on the characterization technologies to conduct experiments  
78 on surfaces and interfaces<sup>19-21</sup> such as Focus Ion Beam Scanning Electron Microscopy (FIB-  
79 SEM),<sup>15,22,23</sup> Transmission Electron Microscopy (TEM),<sup>23,24</sup> Atomic Force Microscopy  
80 (AFM),<sup>16,25,26</sup> X-ray Diffraction (XRD),<sup>27,28</sup> X-ray microtomography (Micro-CT),<sup>29,30</sup> Nuclear  
81 Magnetic Resonance (NMR),<sup>31,32</sup> etc. Implementing these methodologies to characterize  
82 microscopic phenomena becomes challenging at the molecular level. Unlike experiments,  
83 computational simulations can study physical phenomena over a range of scales,<sup>33</sup> directly  
84 connecting the microscopic details of a system to macroscopic properties of experimental  
85 interest.<sup>34</sup> Due to the intensive computation, Quantum Mechanics (QM) simulations have strict  
86 limits on the size, time, and complexity of the systems.<sup>33-35</sup> Molecular simulations, built on  
87 classical molecular mechanics (MM) such as Monte Carlo (MC) and Molecular Dynamics (MD),  
88 are more appropriate than QM methods to address the issues of size and complexity of the

89 hydrocarbon systems. MC methods are stochastic approach, suitable for system equilibrium,  
90 while MD techniques are deterministic, suitable for both equilibrium and transport properties of  
91 a given system.<sup>34,35</sup> Thus, this study used MD to investigate the energetics of fluid-rock  
92 interactions. Currently, there are several studies using MD to investigate hydrocarbon fluid  
93 interactions with kerogen and minerals, such as 1) the adsorption, diffusion, and permeation of  
94 hydrocarbon fluid in shale kerogen and kerogen analogue;<sup>36-43</sup> 2) slippage, displacement, and  
95 adsorption of hydrocarbon flow on quartz, calcite slits, and montmorillonite slits;<sup>44-47</sup> 3)  
96 detachment of oil cluster from silicate surfaces in surfactant solution.<sup>48</sup> These studies evaluated  
97 the effect of nanopores on the properties of hydrocarbon fluid, such as bulk viscosity, contact  
98 angle, and slippage with focuses on the phenomena of the interactions. For instance, Liu et al  
99 2012 stated that water can penetrate the oil—water interface and form a surface water layer on a  
100 hydrophilic silica surface, enhancing the oil detachment from the hydrophilic surface.<sup>48</sup>  
101 However, there is a knowledge gap in the energetic aspect of the interactions, which is  
102 essentially underexplored. This lack of the knowledge on the thermodynamics of the interactions  
103 limits current understanding of the fundamental mechanism in hydrocarbon fluids interactions  
104 with reservoir formations.

105         The present study intends to examine the feasibility of the computational approach to  
106 evaluate the free energy profile of oil compounds desorption from the surfaces of reservoir rock  
107 materials. Umbrella Sampling, widely used in computational biology and biochemistry<sup>49</sup>, was  
108 adopted to compute the free energy profiles of the oil interactions with the rock materials in the  
109 desorption. We studied the surfaces of kerogen and calcite to evaluate the effect of four different  
110 variables including oil polarity (polar vs non-polar oil), oil cluster size (a single molecule oil vs  
111 30 molecules oil cluster), surface hydrophobicity (inorganic calcite mineral vs organic kerogen),

112 and surface water (the presence vs the absence of surface water). Probing the free energy  
113 changes in oil-rock interactions can provide insight into the thermodynamics of the surface  
114 wettability and hydrocarbon behaviors in reservoir formations.

115

## 116 **2 Method**

### 117 2.1 Molecular models for oil, kerogen, and calcite

118 Crude oil is a mixture of a wide range of polar and non-polar compounds with varying  
119 proportions, composition, and molecular weight. Typically, crude oil contains over 45% non-  
120 polar (e.g. alkanes and cycloalkanes) and less than 15% polar species (e.g. N-, S-, O- and metal-  
121 containing compounds).<sup>50,51</sup> Polar components can significantly affect properties of hydrocarbon  
122 fluid in reservoir such as viscosity, contact angle, interfacial activity, emulsion, and chemical  
123 stability.<sup>52-54</sup> The oil-rock interactions are largely attributed by the polar species,<sup>55</sup> particularly in  
124 organic phases which usually retain more polar components than minerals<sup>52</sup>. Thioalkanes are  
125 common sulfur compounds found in crude oils.<sup>56</sup> Crude oil, especially from shale, can has a high  
126 content of light oil (C<sub>1</sub>-C<sub>9</sub>).<sup>57,58</sup> Therefore, we selected 1-octanethiol (C<sub>8</sub>H<sub>18</sub>S) with a dipole  
127 moment of 2.9 D<sup>59</sup> and its non-polar counterpart n-octane (C<sub>8</sub>H<sub>18</sub>) as the models for polar and  
128 nonpolar oil respectively in our simulations as shown in Figure 2. In addition, to model a small  
129 oil drop, we prepared two oil clusters consisted of 30 molecules of octanethiol and octane for  
130 polar and non-polar oil droplets respectively as shown in Figure 3(c).

131 Reservoir rocks have complex microstructures and mineralogy and contains various  
132 amount of inorganic and organic constituents. Major mineral phases include clays, quartz, and  
133 carbonates (calcite and dolomite).<sup>60</sup> Due to its simple structure and ubiquitous presence in



134 formation rocks, the calcite (104) face was chosen as a mode for hydrophilic surface of reservoir  
135 rocks. The calcite (104) is a flat stoichiometric surface. It is one of most common mineral faces  
136 occurred in both geological and biological systems and has been well studied both  
137 computationally and experimentally.<sup>61</sup> The key organic phase in shale involved in the  
138 interactions with hydrocarbon fluid is kerogen.<sup>52,62,63</sup> Despite the complexity of kerogen in  
139 reservoir formations<sup>64</sup>, many studies used graphene to represent kerogen<sup>36,42,43,65–68</sup>. The  
140 differences between graphene and kerogen, such as bonding environment of functional  
141 groups<sup>69,70</sup> and surface morphology<sup>64</sup>, give rise to different chemical and mechanical properties  
142 and interfacial interactions. These deviations can lead to inaccurate modeling with respect to  
143 experimental measurements<sup>70,71</sup>. To capture fundamental properties of kerogen, we employed a  
144 molecular fragment C<sub>22</sub>H<sub>13</sub>ON directly derived from type II kerogen to build kerogen surfaces,<sup>37</sup>  
145 which is the most common kerogen in hydrocarbon-bearing shale formations.<sup>64</sup> The kerogen  
146 molecule has five benzene rings, a secondary amine, and a phenol group, making this kerogen  
147 molecule a polar compound. To create kerogen surfaces, 511 kerogen molecules were randomly  
148 added into a computational supercell (18,907 atoms in total), quenched from 3000 to 300 K. The  
149 surface was then created by inserting a vacuum space between the kerogen and lastly a  
150 stabilization and a relaxation of the surface were followed at 300 K using an NVT ensemble.

151 The calcite (104) surface in Figure 3(b) was built with 1620 CaCO<sub>3</sub> molecule units with a  
152 dimension of approximately 7 × 7 × 2 nm with 8,100 atoms. The kerogen surface in Figure 3(a)  
153 was built with 511 C<sub>22</sub>H<sub>13</sub>ON molecule units with a dimension of approximately 8 × 8 × 3 nm  
154 and 18,907 atoms as shown. Because of the ubiquitous presence of water in the reservoir  
155 formations, water molecules were added to the fluid. To ensure the oil molecules surrounded by  
156 water, 7,250 and 10,000 water molecules were added to the calcite surface of single oil molecule

157 or oil cluster, respectively, while 7,500 and 10,000 water molecules were placed on kerogen  
158 surfaces of single oil molecule or oil cluster, respectively.

159 A previous experimental study indicates the calcite (104) surface exhibits neutral charge  
160 due to the stoichiometry and alternating of  $\text{Ca}^{2+}$  and  $\text{CO}_3^{2-}$ .<sup>72,73</sup> Kerogen surfaces can be  
161 negatively charged due to the deprotonation of functional groups, such as OH and NH. However,  
162 classical MD models only simulate interatomic interactions by empirical potentials for bond  
163 length, angle, and dihedral, whereas formation and breaking of covalent bonds are not considered  
164 unless specified by force field. Both calcite and kerogen surfaces maintain electrical neutrality  
165 owing to the charge balance of each model molecule. Layers of alternating  $\text{Ca}^{2+}$  and  $\text{CO}_3^{2-}$  on the  
166 calcite (104) create a flat surface, while the benzene rings and polar functional groups of kerogen  
167 molecule yield highly heterogenous surfaces of kerogen.

168

## 169 2.2 Molecular Dynamics (MD) Simulation and Gibbs Free Energy Profiles

170 MD simulations in this study were deployed using software package GRONingen  
171 MACHine for Chemical Simulations (GROMACS).<sup>74</sup> All simulations employed three-  
172 dimensional periodic boundary conditions. The OPLS-AA force field was used to describe oil  
173 molecules and kerogen.<sup>75</sup> The SPC potential is used to describe water molecule.<sup>76</sup> A previously  
174 developed force field was used for calcite.<sup>77</sup> All these potentials have been tested and are capable  
175 of producing satisfactory results on bulk and interfacial properties, which are consistent with  
176 experimental data.<sup>78-80</sup> Newton's equations of motion were integrated using the leap-frog scheme  
177 with a timestep of 1 fs, fast Smooth Particle-Mesh Ewald (SPME) electrostatics, Verlet cutoff-  
178 scheme, and temperature coupling using a Nose-Hoover extended ensemble with a coupling

179 constant of 0.1 ps. Simulations were visualized by Visual Molecular Dynamics (VMD)  
180 package.<sup>81</sup>

181 The potential of mean force for the oil interactions with different surfaces was computed  
182 by Umbrella Sampling and the Weighted Histogram Analysis Method (WHAM).<sup>82,83</sup> Gromacs  
183 package was used to carry out Umbrella Sampling simulations by running separate simulation  
184 windows along the reaction coordinate individually. These windows were generated by  
185 extracting a series of configurations from a pulling simulation that drew the oil into or away from  
186 the surfaces along the designated reaction coordinate.

187 In each simulation window, umbrella potential, a biased harmonic potential, was applied  
188 to the system. For each individual simulation window, a constraint potential with a force constant  
189  $9000 \text{ kJ}\cdot\text{mol}^{-1}\cdot\text{nm}^{-1}$  for 0.1 ns to equilibrate the system was first applied, then an umbrella  
190 potential with a force constant  $9000 \text{ kJ}\cdot\text{mol}^{-1}\cdot\text{nm}^{-2}$  was deployed for 0.1 ns up to 0.2 ns to obtain  
191 probability distribution of the given reaction coordinate. With enough sampling overlaps  
192 between simulation windows in the entire reaction coordinate space, a free energy profile curve  
193 can be calculated by combining data from each window using WHAM.<sup>82,84</sup>

194 An analysis routine to estimate the errors of the energy profiles was developed using  
195 LOESS algorithm in RStudio.<sup>85,86</sup> This method took the energy profile and employed the  
196 bootstrap technique to calculate the confidential intervals at 95% confidence level. The  
197 computed errors are listed as shown in Table 1 denoted by brackets. The fluctuation of free  
198 energy profile, as shown in Figure S1, is consistent with the size of the estimated error bar.

199

200 **3 Results**

201 Free energy surfaces in Figures 4-7 show how the system energy changes as a function of  
202 the distance between oil compounds and surfaces. When the oils molecules are close to the  
203 surfaces, the energy increases due to repulsive interactions. When the oils gradually move away  
204 from the surface, the energy first reaches the minimal point, at which the adsorption occurs at the  
205 surfaces. An absence of the minimum suggests zero desorption energy. As the distance  
206 continuously increases, the energy increase until the system reaches the energy plateau where no  
207 additional energy is required to desorb the oil molecules from the surfaces.

208

### 209 3.1 Interactions of oil molecules with kerogen surface

210 The free energy profiles in Figure 4 and Table 1 show the energy changes as a function of  
211 the distance between oil compounds and kerogen surface in the presence of water. The  
212 desorption energies are  $17.0 \pm 2.0$  kJ/mol and  $16.5 \pm 3.3$  kJ/mol for non-polar and polar single  
213 oil molecule and  $371 \pm 12.4$  kJ/mol and  $209 \pm 7.0$  kJ/mol for non-polar and polar oil clusters,  
214 respectively. In the absence of water, it is challenging to maintain oil molecules as a cluster at or  
215 above 300 K. To stabilize the oil cluster, a series of Umbrella Sampling simulations were carried  
216 out under lower system temperatures to extrapolate the desorption energy to 300 K (detail was  
217 discussed in Figure S3). The desorption energies of the oil clusters on kerogen surfaces are  $437 \pm$   
218  $13.5$  kJ/mol for both polar and non-polar (Figure S3). For the single oil molecule, the desorption  
219 energies on kerogen in Figure 5 and Table 1 are  $23.3 \pm 3.5$  kJ/mol and  $39.5 \pm 9.5$  kJ/mol for non-  
220 polar and polar, respectively.

221

### 222 3.2 Interactions of oil molecules with calcite (104) surface

223           The free energy profiles in Figure 6 shows how free energy changes as a function of the  
224 distance between oil compounds and the calcite (104) surface in water. Unlike the rest free  
225 energy profiles (described later), they exhibit a distinct pattern: as the distance increase, the free  
226 energy quickly decreased and then stayed at the same value as the molecule is further away from  
227 the surface. Such patterns indicate near zero energy of the desorption of oil molecules on the  
228 calcite surface in the presence of water.

229           For comparison, the same systems without water were simulated, of which the free  
230 energy profiles are depicted in Figure 7. The results show that  $33.6 \pm 3.9$  kJ/mol and  $18.0 \pm 5.5$   
231 kJ/mol are required to desorb polar and non-polar oil molecules from the calcite surfaces  
232 respectively, and  $222 \pm 36$  kJ/mol and  $198 \pm 42$  kJ/mol to desorb polar and non-polar oil clusters,  
233 respectively. A detailed analysis of the trajectory (Figure S4) suggests that the polar molecule  
234 was bound to the calcite surface through the thiol functional group  $-SH$ , which confirms a  
235 previous study on the adsorption of simple organic molecules on calcite (104).<sup>87</sup> In addition, the  
236 thiol group  $-SH$  of polar oil appears to favor the sites of  $Ca^{2+}$  site of calcite (104) surface,  
237 whereas the non-polar oil shows no preference of absorption sites.

238

## 239 **4 Discussion**

### 240 4.1 Effect of surface composition on the desorption energy

241           Our study shows that, in general, oil molecules have stronger interactions with kerogen  
242 than with calcite regardless of surface environment and oil molecular polarity. Kerogen is an  
243 organic compound and usually oleophilic, whose surface property depends on the specific  
244 functional groups. The kerogen model in this study contains functional groups such as hydroxyl

245 (–OH) and thiol (sulfhydryl, –SH) groups which inherently exhibit a strong affinity with  
246 hydrophilic surfaces while the rest strongly interact with hydrophobic surfaces. On the other  
247 hand, calcite, especially the (104) face, is strongly hydrophilic with ionic species  $\text{Ca}^{2+}$  and  $\text{CO}_3^{2-}$   
248 on the surface. Therefore, water can be more easily desorbed from the kerogen surface than from  
249 the calcite surface, leading to higher desorption energy for oil molecules at the kerogen surface  
250 and weak desorption at the calcite surface. Another factor that contributes to the difference  
251 between kerogen and calcite is the surface area: calcite has a low surface area which weakens its  
252 sorption capacities,<sup>88</sup> whereas kerogen is porous and waxy according to experimental  
253 observations.<sup>64,89</sup> Thus, the effective surface area on kerogen would be much higher than calcite,  
254 leading to a higher desorption capacities for oil.

255         As a result of their different surface properties, the desorption energy at kerogen surface  
256 is higher than at the calcite surface: 5.3 to 17 kJ/mol higher for a single oil molecule and 210 to  
257 372 kJ/mol higher for the oil cluster (7.0 to 12.4 kJ/mol per molecule for the oil cluster). The  
258 difference in the desorption energies of both single molecule oil and oil cluster implies that oil  
259 recovery from organic phases of reservoir rock can take more energy than from these highly  
260 hydrophilic surfaces of inorganic mineral phases such as calcite.

261

## 262 4.2 Effect of molecular polarity

263         Our study shows that the polar oil has a stronger interaction with the kerogen and calcite  
264 surfaces than non-polar oil. At kerogen surface, molecular polarity plays an imperative role in  
265 the energetics of the oil desorption. These phenomena can be explained by the dipole  
266 interactions. Since there is no free ion in the systems, the intermolecular interactions are

267 dominated by permanent dipole interaction, or Keesom interaction. As shown in Figure S5 (a)  
268 and (c), the thiol functional group ( $-SH$ , yellow) of the polar oil tend stay in close proximity to  
269 the functional groups of kerogen molecules such as amine ( $-NH-$ , blue) and hydroxyl ( $-OH$ , red)  
270 upon contact at the interface, which confirms the expected dipole interactions. Unlike the polar  
271 oil, non-polar oil molecules have no dipole moment, therefore a weaker desorption energy than  
272 the polar oil molecules is expected. Thus, the interactions of the polar oil molecule with kerogen  
273 surface is stronger than that of non-polar.<sup>90</sup> As shown in the Table 1, the desorption energies of  
274 the single molecule oil show that the polar oil molecule requires energy about two times of the  
275 energy of non-polar per molecule in the absence of water. The desorption energies of single polar  
276 and nonpolar oil molecules are approximately the same in the presence of water. For the oil  
277 cluster, our calculation indicates that polar oil cluster requires the similar desorption energies as  
278 the non-polar oil cluster. These results suggest that the effect of polarity is complicated by  
279 kerogen surface property and the presence of water.

280 At the calcite (104) surface, polar oil molecules consistently require higher desorption  
281 energies than its counterpart non-polar oil owing to the molecular dipole of the polar oil and the  
282 hydrophilic nature of the calcite surface. Although previous studies suggested that calcite (104)  
283 is overall non-polar because the alternating  $Ca^{2+}$  and  $CO_3^{2-}$  are closely packed and charge  
284 balance is maintained,<sup>91,92</sup> the electrostatic interaction between ionic species at the calcite surface  
285 and the functional group at the polar molecule favors the adsorption of the polar oil molecules.  
286 Therefore, the desorption energy for the polar oil molecule is approximately two times of the  
287 desorption energy for the non-polar oil molecule and the desorption energy for the polar oil  
288 molecular cluster is approximately 10% higher than the desorption energy for the non-polar oil  
289 cluster in the absence of water.

290  
291  
292  
293  
294  
295  
296  
297  
298  
299  
300  
301  
302  
303  
304  
305  
306  
307  
308  
309  
310  
311

#### 4.3 Effect of surface water

Our study shows that the presence of surface water reduces the oil desorption energy on all surface conditions, promoting oil desorption in all these cases. As discussed previously, the calcite surface is hydrophilic, while kerogen is both hydrophilic and hydrophobic. The surface water can easily be attracted to the calcite surface and kerogen hydrophilic functional groups. Both water and polar oil molecules have similar dipole moments 2.9 D and 2.27 D,<sup>59,76</sup> respectively. Water molecules compete with polar oil molecules for adsorption at surfaces with a hydrophilic character, and consequently reducing the desorption energy of the oil molecules at the surfaces. The interactions of waters with the calcite (104) surfaces were much stronger than with kerogen surfaces, suggesting a weaker hydrophilic nature of kerogen surface than the calcite surface. The affinity between calcite and water is stronger than that between calcite and oil, resulting in a strong oil-repellent surface of calcite in the presence of water. As shown in Table 1, kerogen surface with water requires much lower energies to desorb oil. For polar oil, the surface water brought a reduction of 50% - 60% on desorption energy to desorb polar oil compound and 15% - 30% reduction for non-polar oil compound. The energy differences between non-polar and polar oil also demonstrate the crucial role of molecular polarity on the fluid-rock interactions. Given the strong hydrophilicity of calcite, the calcite surface becomes oleophobic, jettisoned all the surface oil, in the presence of water. The result provides a fundamental understanding of the role of water in interactions of oil molecules and reservoir materials and in oil recovery.



312 4.4 Effect of oil clustering

313 Our study shows that oil clusters require lower desorption energies per molecule than a  
314 single oil molecule. For instance, the desorption energy of a single molecule of polar oil is 4.6 to  
315 25.2 kJ/mol higher than the desorption energy per molecule of the oil cluster, which is an  
316 increase of 37% to 340% of desorption energy per molecule in the oil cluster. This difference is  
317 mainly caused by the number of oil molecules that directly interact with the surface. Not all the  
318 molecules in the 30-molecule clusters directly interact with the surfaces, while the single  
319 molecule always interacts with the surfaces, which leads to the smaller desorption energies per  
320 molecule of a molecular cluster. Although the oil molecular clusters are too small to be  
321 comparable with oils in the porous medium in reservoir rocks, the trend quantified in this study  
322 suggests that as the pore size decreases, recovering the oil confined in the pores becomes more  
323 challenging.

324

325 **5 Concluding remarks and implications**

326 This study demonstrated that Molecular Dynamics simulation is capable of calculating  
327 the free energy surface of desorption of single oil molecules and oil molecular clusters at calcite  
328 and kerogen surfaces. The results provide fundamental understandings of the interfacial  
329 interactions and valuable implications for oil recovery in reservoirs. The main conclusions are as  
330 follows.

331 (1) Hydrophobicity of the surface of reservoir materials has a significant effect on the  
332 desorption of the oil molecules from the surfaces, leading to a higher free energy cost for

333 oil displacement from organic phases of reservoir rock than from the highly hydrophilic  
334 surfaces of inorganic mineral phases such as calcite.

335 (2) The polarity of oil molecules strongly affects the interfacial interactions at both the  
336 kerogen and calcite surfaces. The polar oil molecules require more energy to be  
337 recovered from both surfaces than non-polar ones. For complex hydrocarbon fluid  
338 systems, having a large portion of polar compounds in the oil poses a great challenge. In  
339 order to effectively model the interactions between oil and the reservoir materials and to  
340 produce reliable results, an accurate description of the polarity of oil molecules is  
341 necessary.

342 (3) The presence of water at interface plays a fundamental role in the interactions  
343 between oil molecules and reservoir materials. Because of its large dipole moment, water  
344 facilitates the oil desorption by interacting with hydrophilic surfaces or sites of either  
345 organic kerogen or inorganic minerals.

346 (4) Single oil molecule or small oil molecule cluster dispersed in small nanopores tend to  
347 be more challenging to be recovered than large oil molecular clusters due to the stronger  
348 interactions of oil molecules with the surfaces.

349 The success of implementing the free energy methods to study the simple hydrocarbon  
350 fluid systems paves the way for building more realistic simulations for complex systems by  
351 varying temperatures, adding fluid components (e.g. electrolytes, methane, carbon dioxide, and  
352 large oil compounds) and introducing other major inorganic phases such as clay minerals and  
353 quartz.

354

355 **Conflicts of interest**

356 There are no conflicts to declare.

357

358 **Acknowledgements**

359 This research used resources of the National Energy Research Scientific Computing  
360 Center (NERSC), a U.S. Department of Energy Office of Science User Facility operated  
361 under Contract No. DE-AC02-05CH11231. Portions of this research were conducted  
362 with high performance computing resources provided by Louisiana State University  
363 (<http://www.hpc.lsu.edu>).

## 364 References

- 365 (1) EIA. *Annual Energy Outlook 2019*; AEO2019; U.S. Energy Information Administration: Washington,  
366 DC, 2019.
- 367 (2) Thomas, S. Enhanced Oil Recovery - An Overview. *Oil Gas Sci. Technol. - Rev. IFP* **2008**, *63* (1), 9–19.  
368 <https://doi.org/10.2516/ogst:2007060>.
- 369 (3) Forbes, P. The Status of Core Analysis. *J. Pet. Sci. Eng.* **1998**, *19* (1), 1–6.  
370 [https://doi.org/10.1016/S0920-4105\(97\)00030-2](https://doi.org/10.1016/S0920-4105(97)00030-2).
- 371 (4) Gao, B.; Kralik, J.; Vo, L.; Shebl, H.; Al Shehhi, R.; Al Jawhari, M. O.; Fullmer, S. State of the Art  
372 Special Core Analysis Program Design and Results for a Middle Eastern Carbonate Reservoir;  
373 Society of Petroleum Engineers, 2015. <https://doi.org/10.2118/177510-MS>.
- 374 (5) van der Weerd, H.; Masalmeh, S. K.; Jing, X. D.; van Vark, W.; Christiansen, S.; Van Dorp, J. Impact  
375 of SCAL (Special Core Analysis) on Carbonate Reservoirs: How Capillary Forces Can Affect Field  
376 Performance Predictions. *Petrophysics* **2004**, *45* (05).
- 377 (6) Cueto-Felgueroso, L.; Juanes, R. Forecasting Long-Term Gas Production from Shale. *Proc. Natl.*  
378 *Acad. Sci.* **2013**, *110* (49), 19660. <https://doi.org/10.1073/pnas.1319578110>.
- 379 (7) Zhang, T.; Ellis, G. S.; Ruppel, S. C.; Milliken, K.; Yang, R. Effect of Organic-Matter Type and Thermal  
380 Maturity on Methane Adsorption in Shale-Gas Systems. *Org. Geochem.* **2012**, *47*, 120–131.  
381 <https://doi.org/10.1016/j.orggeochem.2012.03.012>.
- 382 (8) Hutton, A. C.; Kantsler, A. J.; Cook, A. C.; McKirdy, D. M. ORGANIC MATTER IN OIL SHALES. *APPEA J.*  
383 **1980**, *20* (1), 44–67. <https://doi.org/10.1071/aj79005>.
- 384 (9) Ross, D. J. K.; Marc Bustin, R. The Importance of Shale Composition and Pore Structure upon Gas  
385 Storage Potential of Shale Gas Reservoirs. *Mar. Pet. Geol.* **2009**, *26* (6), 916–927.  
386 <https://doi.org/10.1016/j.marpetgeo.2008.06.004>.
- 387 (10) Loucks, R. G.; Reed, R. M.; Ruppel, S. C.; Hammes, U. Spectrum of Pore Types and Networks in  
388 Mudrocks and a Descriptive Classification for Matrix-Related Mudrock Pores Spectrum of Pore  
389 Types and Networks In Mudrocks. *AAPG Bull.* **2012**, *96* (6), 1071–1098.  
390 <https://doi.org/10.1306/08171111061>.
- 391 (11) Sondergeld, C. H.; Ambrose, R. J.; Rai, C. S.; Moncrieff, J. Micro-Structural Studies of Gas Shales;  
392 Society of Petroleum Engineers, 2010. <https://doi.org/10.2118/131771-MS>.
- 393 (12) Clarkson, C. R.; Solano, N.; Bustin, R. M.; Bustin, A. M. M.; Chalmers, G. R. L.; He, L.; Melnichenko,  
394 Y. B.; Radliński, A. P.; Blach, T. P. Pore Structure Characterization of North American Shale Gas  
395 Reservoirs Using USANS/SANS, Gas Adsorption, and Mercury Intrusion. *Fuel* **2013**, *103*, 606–616.  
396 <https://doi.org/10.1016/j.fuel.2012.06.119>.
- 397 (13) Passey, Q. R.; Bohacs, K.; Esch, W. L.; Klimentidis, R.; Sinha, S. From Oil-Prone Source Rock to Gas-  
398 Producing Shale Reservoir - Geologic and Petrophysical Characterization of Unconventional Shale  
399 Gas Reservoirs; Society of Petroleum Engineers, 2010. <https://doi.org/10.2118/131350-MS>.
- 400 (14) Vernik, L.; Milovac, J. Rock Physics of Organic Shales. *Lead. Edge* **2011**, *30* (3), 318–323.  
401 <https://doi.org/10.1190/1.3567263>.
- 402 (15) Milliken, K. L.; Rudnicki, M.; Awwiller, D. N.; Zhang, T. Organic Matter–Hosted Pore System,  
403 Marcellus Formation (Devonian), Pennsylvania Geohorizon. *AAPG Bull.* **2013**, *97* (2), 177–200.  
404 <https://doi.org/10.1306/07231212048>.
- 405 (16) Shabro, V.; Torres-Verdin, C.; Javadpour, F. Numerical Simulation of Shale-Gas Production: From  
406 Pore-Scale Modeling of Slip-Flow, Knudsen Diffusion, and Langmuir Desorption to Reservoir  
407 Modeling of Compressible Fluid; Society of Petroleum Engineers, 2011.  
408 <https://doi.org/10.2118/144355-MS>.

- 409 (17) Wu, K.; Li, X.; Wang, C.; Yu, W.; Chen, Z. Model for Surface Diffusion of Adsorbed Gas in Nanopores  
410 of Shale Gas Reservoirs. *Ind. Eng. Chem. Res.* **2015**, *54* (12), 3225–3236.  
411 <https://doi.org/10.1021/ie504030v>.
- 412 (18) Wang, F. P.; Reed, R. M. Pore Networks and Fluid Flow in Gas Shales; Society of Petroleum  
413 Engineers, 2009. <https://doi.org/10.2118/124253-MS>.
- 414 (19) Zaera, F. Probing Liquid/Solid Interfaces at the Molecular Level. *Chem. Rev.* **2012**, *112* (5), 2920–  
415 2986. <https://doi.org/10.1021/cr2002068>.
- 416 (20) *Surface Analysis Methods in Materials Science*; O'Connor, J., Sexton, B., Smart, R., Eds.; Springer  
417 Series in Surface Sciences; Springer-Verlag: Berlin Heidelberg, 1992.
- 418 (21) Mineralogical Society of America - Mineral-Water Interface Geochemistry  
419 <http://www.minsocam.org/msa/rim/rim23.html> (accessed Mar 13, 2019).
- 420 (22) Milner, M.; McLin, R.; Petriello, J. Imaging Texture and Porosity in Mudstones and Shales:  
421 Comparison of Secondary and Ion-Milled Backscatter SEM Methods; Society of Petroleum  
422 Engineers, 2010. <https://doi.org/10.2118/138975-MS>.
- 423 (23) Curtis, M. E.; Ambrose, R. J.; Sondergeld, C. H.; Rai, C. S. Transmission and Scanning Electron  
424 Microscopy Investigation of Pore Connectivity of Gas Shales on the Nanoscale; Society of  
425 Petroleum Engineers, 2011. <https://doi.org/10.2118/144391-MS>.
- 426 (24) Bernard, S.; Horsfield, B.; Schulz, H.-M.; Wirth, R.; Schreiber, A.; Sherwood, N. Geochemical  
427 Evolution of Organic-Rich Shales with Increasing Maturity: A STXM and TEM Study of the Posidonia  
428 Shale (Lower Toarcian, Northern Germany). *Mar. Pet. Geol.* **2012**, *31* (1), 70–89.  
429 <https://doi.org/10.1016/j.marpetgeo.2011.05.010>.
- 430 (25) Javadpour, F. Nanopores and Apparent Permeability of Gas Flow in Mudrocks (Shales and  
431 Siltstone). *J. Can. Pet. Technol.* **2009**, *48* (08), 16–21. <https://doi.org/10.2118/09-08-16-DA>.
- 432 (26) Javadpour, F.; Moravvej Farshi, M.; Amrein, M. Atomic-Force Microscopy: A New Tool for Gas-  
433 Shale Characterization. *J. Can. Pet. Technol.* **2012**, *51* (04), 236–243.  
434 <https://doi.org/10.2118/161015-PA>.
- 435 (27) Bhargava, S.; Awaja, F.; Subasinghe, N. D. Characterisation of Some Australian Oil Shale Using  
436 Thermal, X-Ray and IR Techniques. *Fuel* **2005**, *84* (6), 707–715.  
437 <https://doi.org/10.1016/j.fuel.2004.11.013>.
- 438 (28) Elgmati, M. M.; Zhang, H.; Bai, B.; Flori, R. E.; Qu, Q. Submicron-Pore Characterization of Shale Gas  
439 Plays; Society of Petroleum Engineers, 2011. <https://doi.org/10.2118/144050-MS>.
- 440 (29) Tiwari, P.; Deo, M.; Lin, C. L.; Miller, J. D. Characterization of Oil Shale Pore Structure before and  
441 after Pyrolysis by Using X-Ray Micro CT. *Fuel* **2013**, *107*, 547–554.  
442 <https://doi.org/10.1016/j.fuel.2013.01.006>.
- 443 (30) Dului, O. G. Computer Axial Tomography in Geosciences: An Overview. *Earth-Sci. Rev.* **1999**, *48* (4),  
444 265–281. [https://doi.org/10.1016/S0012-8252\(99\)00056-2](https://doi.org/10.1016/S0012-8252(99)00056-2).
- 445 (31) Kadayam Viswanathan, R. K.; Cao Minh, C.; Zielinski, L.; Vissapragada, B.; Akkurt, R.; Song, Y.-Q.;  
446 Liu, C.; Jones, S.; Blair, E. Characterization of Gas Dynamics in Kerogen Nanopores by NMR; Society  
447 of Petroleum Engineers, 2011. <https://doi.org/10.2118/147198-MS>.
- 448 (32) Korb, J.-P.; Nicot, B.; Louis-Joseph, A.; Bubici, S.; Ferrante, G. Dynamics and Wettability of Oil and  
449 Water in Oil Shales. *J. Phys. Chem. C* **2014**, *118* (40), 23212–23218.  
450 <https://doi.org/10.1021/jp508659e>.
- 451 (33) Cygan, R. T. Molecular Modeling in Mineralogy and Geochemistry. *Rev. Mineral. Geochem.* **2001**,  
452 *42* (1), 1–35. <https://doi.org/10.2138/rmg.2001.42.1>.
- 453 (34) Allen, M.; Tildesley, D. *Computer Simulation of Liquids*, Second Edition.; Oxford University Press:  
454 Oxford, New York, 2017.
- 455 (35) Frenkel, D.; Smit, B. *Understanding Molecular Simulation: From Algorithms to Applications*, Second  
456 Edition.; Academic Press: San Diego, 2002.

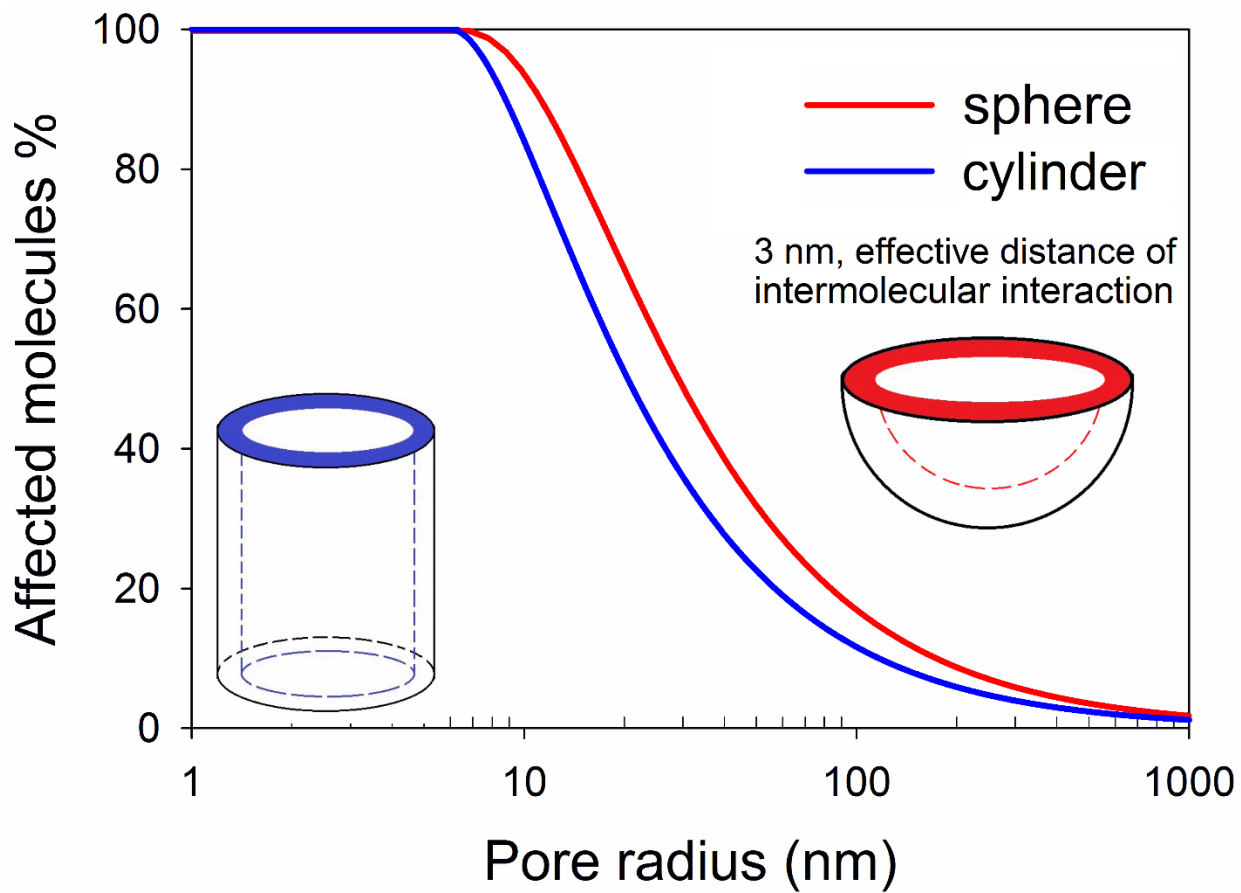
- 457 (36) Falk, K.; Coasne, B.; Pellenq, R.; Ulm, F.-J.; Bocquet, L. Subcontinuum Mass Transport of Condensed  
458 Hydrocarbons in Nanoporous Media. *Nat. Commun.* **2015**, *6*, 6949.  
459 <https://doi.org/10.1038/ncomms7949>.
- 460 (37) Collell, J.; Galliero, G.; Gouth, F.; Montel, F.; Pujol, M.; Ungerer, P.; Yiannourakou, M. Molecular  
461 Simulation and Modelisation of Methane/Ethane Mixtures Adsorption onto a Microporous  
462 Molecular Model of Kerogen under Typical Reservoir Conditions. *Microporous Mesoporous Mater.*  
463 **2014**, *197*, 194–203. <https://doi.org/10.1016/j.micromeso.2014.06.016>.
- 464 (38) Collell, J.; Galliero, G.; Vermorel, R.; Ungerer, P.; Yiannourakou, M.; Montel, F.; Pujol, M. Transport  
465 of Multicomponent Hydrocarbon Mixtures in Shale Organic Matter by Molecular Simulations. *J.*  
466 *Phys. Chem. C* **2015**, *119* (39), 22587–22595. <https://doi.org/10.1021/acs.jpcc.5b07242>.
- 467 (39) Collell, J.; Ungerer, P.; Galliero, G.; Yiannourakou, M.; Montel, F.; Pujol, M. Molecular Simulation of  
468 Bulk Organic Matter in Type II Shales in the Middle of the Oil Formation Window. *Energy Fuels*  
469 **2014**, *28* (12), 7457–7466. <https://doi.org/10.1021/ef5021632>.
- 470 (40) Sui, H.; Yao, J. Effect of Surface Chemistry for CH<sub>4</sub>/CO<sub>2</sub> Adsorption in Kerogen: A Molecular  
471 Simulation Study. *J. Nat. Gas Sci. Eng.* **2016**, *31*, 738–746.  
472 <https://doi.org/10.1016/j.jngse.2016.03.097>.
- 473 (41) Yiannourakou, M.; Ungerer, P.; Leblanc, B.; Rozanska, X.; Saxe, P.; Vidal-Gilbert, S.; Gouth, F.;  
474 Montel, F. Molecular Simulation of Adsorption in Microporous Materials. *Oil Gas Sci. Technol. –*  
475 *Rev. D'IFP Energ. Nouv.* **2013**, *68* (6), 977–994. <https://doi.org/10.2516/ogst/2013134>.
- 476 (42) Lee, T.; Bocquet, L.; Coasne, B. Activated Desorption at Heterogeneous Interfaces and Long-Time  
477 Kinetics of Hydrocarbon Recovery from Nanoporous Media. *Nat. Commun.* **2016**, *7*, 11890.  
478 <https://doi.org/10.1038/ncomms11890>.
- 479 (43) Ambrose, R. J.; Hartman, R. C.; Diaz-Campos, M.; Akkutlu, I. Y.; Sondergeld, C. H. Shale Gas-in-Place  
480 Calculations Part I: New Pore-Scale Considerations. *SPE J.* **2012**, *17* (01), 219–229.  
481 <https://doi.org/10.2118/131772-PA>.
- 482 (44) Wang, S.; Javadpour, F.; Feng, Q. Molecular Dynamics Simulations of Oil Transport through  
483 Inorganic Nanopores in Shale. *Fuel* **2016**, *171*, 74–86. <https://doi.org/10.1016/j.fuel.2015.12.071>.
- 484 (45) Wang, S.; Feng, Q.; Javadpour, F.; Yang, Y.-B. Breakdown of Fast Mass Transport of Methane  
485 through Calcite Nanopores. *J. Phys. Chem. C* **2016**, *120* (26), 14260–14269.  
486 <https://doi.org/10.1021/acs.jpcc.6b05511>.
- 487 (46) Zheng, H.; Du, Y.; Xue, Q.; Zhu, L.; Li, X.; Lu, S.; Jin, Y. Surface Effect on Oil Transportation in  
488 Nanochannel: A Molecular Dynamics Study. *Nanoscale Res. Lett.* **2017**, *12* (1), 413.  
489 <https://doi.org/10.1186/s11671-017-2161-2>.
- 490 (47) Underwood, T.; Erastova, V.; Cubillas, P.; Greenwell, H. C. Molecular Dynamic Simulations of  
491 Montmorillonite–Organic Interactions under Varying Salinity: An Insight into Enhanced Oil  
492 Recovery. *J. Phys. Chem. C* **2015**, *119* (13), 7282–7294. <https://doi.org/10.1021/acs.jpcc.5b00555>.
- 493 (48) Liu, Q.; Yuan, S.; Yan, H.; Zhao, X. Mechanism of Oil Detachment from a Silica Surface in Aqueous  
494 Surfactant Solutions: Molecular Dynamics Simulations. *J. Phys. Chem. B* **2012**, *116* (9), 2867–2875.  
495 <https://doi.org/10.1021/jp2118482>.
- 496 (49) Kästner, J. Umbrella Sampling. *Wiley Interdiscip. Rev. Comput. Mol. Sci.* **2011**, *1* (6), 932–942.  
497 <https://doi.org/10.1002/wcms.66>.
- 498 (50) Hughey, C. A.; Rodgers, R. P.; Marshall, A. G.; Qian, K.; Robbins, W. K. Identification of Acidic NSO  
499 Compounds in Crude Oils of Different Geochemical Origins by Negative Ion Electrospray Fourier  
500 Transform Ion Cyclotron Resonance Mass Spectrometry. *Org. Geochem.* **2002**, *33* (7), 743–759.  
501 [https://doi.org/10.1016/S0146-6380\(02\)00038-4](https://doi.org/10.1016/S0146-6380(02)00038-4).
- 502 (51) Hyne, N. J. *Nontechnical Guide to Petroleum Geology, Exploration, Drilling, and Production*;  
503 PennWell Corporation: Tulsa, Okla., 2012.

- 504 (52) Jarvie, D. M. Shale Resource Systems for Oil and Gas: Part 2—Shale-Oil Resource Systems. **2012**,  
505 89–119. <https://doi.org/10.1306/13321447M973489>.
- 506 (53) Buckley, J. S.; Liu, Y.; Monsterleet, S. Mechanisms of Wetting Alteration by Crude Oils. *SPE J.* **1998**,  
507 3 (01), 54–61. <https://doi.org/10.2118/37230-PA>.
- 508 (54) Sayyouh, M. H.; Hemeida, A. M.; Al-Blehed, M. S.; Desouky, S. M. Role of Polar Compounds in  
509 Crude Oils on Rock Wettability. *J. Pet. Sci. Eng.* **1991**, 6 (3), 225–233.  
510 [https://doi.org/10.1016/0920-4105\(91\)90015-F](https://doi.org/10.1016/0920-4105(91)90015-F).
- 511 (55) Speight, J. G. The Chemical and Physical Structure of Petroleum: Effects on Recovery Operations. *J.*  
512 *Pet. Sci. Eng.* **1999**, 22 (1), 3–15. [https://doi.org/10.1016/S0920-4105\(98\)00051-5](https://doi.org/10.1016/S0920-4105(98)00051-5).
- 513 (56) Composition, Classification, and Properties of Petroleum. In *Chemistry of Fossil Fuels and Biofuels*;  
514 Schobert, H., Ed.; Cambridge Series in Chemical Engineering; Cambridge University Press:  
515 Cambridge, 2013; pp 174–191. <https://doi.org/10.1017/CBO9780511844188.012>.
- 516 (57) Mango, F. D. The Light Hydrocarbons in Petroleum: A Critical Review. *Org. Geochem.* **1997**, 26 (7),  
517 417–440. [https://doi.org/10.1016/S0146-6380\(97\)00031-4](https://doi.org/10.1016/S0146-6380(97)00031-4).
- 518 (58) Yanik, J.; Yüksel, M.; Sağlam, M.; Olukçu, N.; Bartle, K.; Frere, B. Characterization of the Oil  
519 Fractions of Shale Oil Obtained by Pyrolysis and Supercritical Water Extraction. *Fuel* **1995**, 74 (1),  
520 46–50. [https://doi.org/10.1016/0016-2361\(94\)P4329-Z](https://doi.org/10.1016/0016-2361(94)P4329-Z).
- 521 (59) Kvashnin, D. G.; Antipina, L. Y.; Sorokin, P. B.; Tenne, R.; Golberg, D. Theoretical Aspects of WS2  
522 Nanotube Chemical Unzipping. *Nanoscale* **2014**, 6 (14), 8400–8404.  
523 <https://doi.org/10.1039/C4NR00437J>.
- 524 (60) Folk, R. L. *Petrology of Sedimentary Rocks*; Hemphill Publishing Company, 1980.
- 525 (61) Kerisit, S.; Parker, S. C. Free Energy of Adsorption of Water and Metal Ions on the {1014} Calcite  
526 Surface. *J. Am. Chem. Soc.* **2004**, 126 (32), 10152–10161. <https://doi.org/10.1021/ja0487776>.
- 527 (62) Curtis, J. B. Fractured Shale-Gas Systems. *AAPG Bull.* **2002**, 86 (11), 1921–1938.  
528 <https://doi.org/10.1306/61EEDDBE-173E-11D7-8645000102C1865D>.
- 529 (63) Jarvie, D. M.; Hill, R. J.; Ruble, T. E.; Pollastro, R. M. Unconventional Shale-Gas Systems: The  
530 Mississippian Barnett Shale of North-Central Texas as One Model for Thermogenic Shale-Gas  
531 Assessment. *AAPG Bull.* **2007**, 91 (4), 475–499. <https://doi.org/10.1306/12190606068>.
- 532 (64) Vandenbroucke, M.; Largeau, C. Kerogen Origin, Evolution and Structure. *Org. Geochem.* **2007**, 38  
533 (5), 719–833. <https://doi.org/10.1016/j.orggeochem.2007.01.001>.
- 534 (65) Hu, Y.; Devegowda, D.; Striolo, A.; Phan, A.; Ho, T. A.; Civan, F.; Sigal, R. F. Microscopic Dynamics of  
535 Water and Hydrocarbon in Shale-Kerogen Pores of Potentially Mixed Wettability. *SPE J.* **2014**, 20  
536 (01), 112–124. <https://doi.org/10.2118/167234-PA>.
- 537 (66) Firouzi, M.; Rupp, E. C.; Liu, C. W.; Wilcox, J. Molecular Simulation and Experimental  
538 Characterization of the Nanoporous Structures of Coal and Gas Shale. *Int. J. Coal Geol.* **2014**, 121,  
539 123–128. <https://doi.org/10.1016/j.coal.2013.11.003>.
- 540 (67) Falk, K.; Pellenq, R.; Ulm, F. J.; Coasne, B. Effect of Chain Length and Pore Accessibility on Alkane  
541 Adsorption in Kerogen. *Energy Fuels* **2015**, 29 (12), 7889–7896.  
542 <https://doi.org/10.1021/acs.energyfuels.5b02015>.
- 543 (68) Ambrose, R. J.; Hartman, R. C.; Diaz Campos, M.; Akkutlu, I. Y.; Sondergeld, C. New Pore-Scale  
544 Considerations for Shale Gas in Place Calculations; Society of Petroleum Engineers, 2010.  
545 <https://doi.org/10.2118/131772-MS>.
- 546 (69) Orendt, A. M.; Pimienta, I. S. O.; Badu, S. R.; Solum, M. S.; Pugmire, R. J.; Facelli, J. C.; Locke, D. R.;  
547 Chapman, K. W.; Chupas, P. J.; Winans, R. E. Three-Dimensional Structure of the Siskin Green River  
548 Oil Shale Kerogen Model: A Comparison between Calculated and Observed Properties. *Energy*  
549 *Fuels* **2013**, 27 (2), 702–710. <https://doi.org/10.1021/ef3017046>.

- 550 (70) Bousige, C.; Ghimbeu, C. M.; Vix-Guterl, C.; Pomerantz, A. E.; Suleimenova, A.; Vaughan, G.;  
551 Garbarino, G.; Feygenson, M.; Wildgruber, C.; Ulm, F.-J.; et al. Realistic Molecular Model of  
552 Kerogen's Nanostructure. *Nat. Mater.* **2016**, *15* (5), 576–582. <https://doi.org/10.1038/nmat4541>.
- 553 (71) Pei, Q.-X.; Zhang, Y.-W.; Shenoy, V. B. Mechanical Properties of Methyl Functionalized Graphene: A  
554 Molecular Dynamics Study. *Nanotechnology* **2010**, *21* (11), 115709. <https://doi.org/10.1088/0957-4484/21/11/115709>.
- 556 (72) Lee, S. S.; Heberling, F.; Sturchio, N. C.; Eng, P. J.; Fenter, P. Surface Charge of the Calcite (104)  
557 Terrace Measured by Rb<sup>+</sup> Adsorption in Aqueous Solutions Using Resonant Anomalous X-Ray  
558 Reflectivity. *J. Phys. Chem. C* **2016**, *120* (28), 15216–15223.  
559 <https://doi.org/10.1021/acs.jpcc.6b04364>.
- 560 (73) Wolthers, M.; Tommaso, D. D.; Du, Z.; Leeuw, N. H. de. Calcite Surface Structure and Reactivity:  
561 Molecular Dynamics Simulations and Macroscopic Surface Modelling of the Calcite–Water  
562 Interface. *Phys. Chem. Chem. Phys.* **2012**, *14* (43), 15145–15157.  
563 <https://doi.org/10.1039/C2CP42290E>.
- 564 (74) Berendsen, H. J. C.; van der Spoel, D.; van Drunen, R. GROMACS: A Message-Passing Parallel  
565 Molecular Dynamics Implementation. *Comput. Phys. Commun.* **1995**, *91* (1), 43–56.  
566 [https://doi.org/10.1016/0010-4655\(95\)00042-E](https://doi.org/10.1016/0010-4655(95)00042-E).
- 567 (75) Robertson, M. J.; Tirado-Rives, J.; Jorgensen, W. L. Improved Peptide and Protein Torsional  
568 Energetics with the OPLS-AA Force Field. *J. Chem. Theory Comput.* **2015**, *11* (7), 3499–3509.  
569 <https://doi.org/10.1021/acs.jctc.5b00356>.
- 570 (76) Berendsen, H. J. C.; Postma, J. P. M.; van Gunsteren, W. F.; Hermans, J. Interaction Models for  
571 Water in Relation to Protein Hydration. In *Intermolecular Forces: Proceedings of the Fourteenth*  
572 *Jerusalem Symposium on Quantum Chemistry and Biochemistry Held in Jerusalem, Israel, April 13–*  
573 *16, 1981*; Pullman, B., Ed.; The Jerusalem Symposia on Quantum Chemistry and Biochemistry;  
574 Springer Netherlands: Dordrecht, 1981; pp 331–342. [https://doi.org/10.1007/978-94-015-7658-1\\_21](https://doi.org/10.1007/978-94-015-7658-1_21).
- 576 (77) Raiteri, P.; Gale, J. D.; Quigley, D.; Rodger, P. M. Derivation of an Accurate Force-Field for  
577 Simulating the Growth of Calcium Carbonate from Aqueous Solution: A New Model for the  
578 Calcite–Water Interface. *J. Phys. Chem. C* **2010**, *114* (13), 5997–6010.  
579 <https://doi.org/10.1021/jp910977a>.
- 580 (78) Geissbühler, P.; Fenter, P.; DiMasi, E.; Srajer, G.; Sorensen, L. B.; Sturchio, N. C. Three-Dimensional  
581 Structure of the Calcite–Water Interface by Surface X-Ray Scattering. *Surf. Sci.* **2004**, *573* (2), 191–  
582 203. <https://doi.org/10.1016/j.susc.2004.09.036>.
- 583 (79) Wolf, G.; Lerchner, J.; Schmidt, H.; Gamsjäger, H.; Königsberger, E.; Schmidt, P. Thermodynamics of  
584 CaCO<sub>3</sub> Phase Transitions. *J. Therm. Anal. Calorim.* **1996**, *46* (2), 353–359.  
585 <https://doi.org/10.1007/BF02135013>.
- 586 (80) Wolf, G.; Königsberger, E.; Schmidt, H. G.; Königsberger, L.-C.; Gamsjäger, H. Thermodynamic  
587 Aspects of the Vaterite–Calcite Phase Transition. *J. Therm. Anal. Calorim.* **2000**, *60* (2), 463–472.  
588 <https://doi.org/10.1023/A:1010114131577>.
- 589 (81) Humphrey, W.; Dalke, A.; Schulten, K. VMD: Visual Molecular Dynamics. *J. Mol. Graph.* **1996**, *14*  
590 (1), 33–38. [https://doi.org/10.1016/0263-7855\(96\)00018-5](https://doi.org/10.1016/0263-7855(96)00018-5).
- 591 (82) Kumar, S.; Rosenberg, J. M.; Bouzida, D.; Swendsen, R. H.; Kollman, P. A. THE Weighted Histogram  
592 Analysis Method for Free-Energy Calculations on Biomolecules. I. The Method. *J. Comput. Chem.*  
593 **1992**, *13* (8), 1011–1021. <https://doi.org/10.1002/jcc.540130812>.
- 594 (83) Roux, B. The Calculation of the Potential of Mean Force Using Computer Simulations. *Comput.*  
595 *Phys. Commun.* **1995**, *91* (1), 275–282. [https://doi.org/10.1016/0010-4655\(95\)00053-I](https://doi.org/10.1016/0010-4655(95)00053-I).



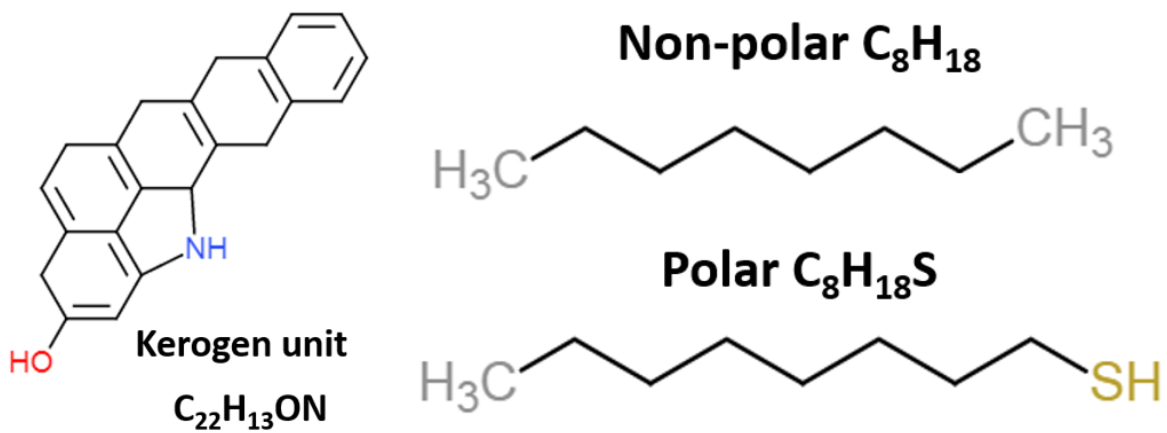
- 596 (84) Hub, J. S.; de Groot, B. L.; van der Spoel, D. G\_wham—A Free Weighted Histogram Analysis  
597 Implementation Including Robust Error and Autocorrelation Estimates. *J. Chem. Theory Comput.*  
598 **2010**, *6* (12), 3713–3720. <https://doi.org/10.1021/ct100494z>.
- 599 (85) Cleveland, W. S. Robust Locally Weighted Regression and Smoothing Scatterplots. *J. Am. Stat.*  
600 *Assoc.* **1979**, *74* (368), 829–836. <https://doi.org/10.1080/01621459.1979.10481038>.
- 601 (86) R Core Team. *R: A Language and Environment for Statistical Computing*; R Foundation for  
602 Statistical Computing: Vienna, Austria, 2019.
- 603 (87) Hakim, S. S.; Olsson, M. H. M.; Sørensen, H. O.; Bovet, N.; Bohr, J.; Feidenhans'l, R.; Stipp, S. L. S.  
604 Interactions of the Calcite {10.4} Surface with Organic Compounds: Structure and Behaviour at  
605 Mineral – Organic Interfaces. *Sci. Rep.* **2017**, *7* (1), 7592. [https://doi.org/10.1038/s41598-017-](https://doi.org/10.1038/s41598-017-06977-4)  
606 [06977-4](https://doi.org/10.1038/s41598-017-06977-4).
- 607 (88) Ross, D. J. K.; Bustin, R. M. Shale Gas Potential of the Lower Jurassic Gordondale Member,  
608 Northeastern British Columbia, Canada. *Bull. Can. Pet. Geol.* **2007**, *55* (1), 51–75.  
609 <https://doi.org/10.2113/gscpgbull.55.1.51>.
- 610 (89) Loucks, R. G.; Reed, R. M.; Ruppel, S. C.; Jarvie, D. M. Morphology, Genesis, and Distribution of  
611 Nanometer-Scale Pores in Siliceous Mudstones of the Mississippian Barnett Shale. *J. Sediment. Res.*  
612 **2009**, *79* (12), 848–861. <https://doi.org/10.2110/jsr.2009.092>.
- 613 (90) Madsen, L.; Grahl-Madsen, L.; Grøn, C.; Lind, I.; Engell, J. Adsorption of Polar Aromatic  
614 Hydrocarbons on Synthetic Calcite. *Org. Geochem.* **1996**, *24* (12), 1151–1155.  
615 [https://doi.org/10.1016/S0146-6380\(96\)00096-4](https://doi.org/10.1016/S0146-6380(96)00096-4).
- 616 (91) García Carmona, J.; Gómez Morales, J.; Rodríguez Clemente, R. Rhombohedral–Scalenohedral  
617 Calcite Transition Produced by Adjusting the Solution Electrical Conductivity in the System  
618 Ca(OH)<sub>2</sub>–CO<sub>2</sub>–H<sub>2</sub>O. *J. Colloid Interface Sci.* **2003**, *261* (2), 434–440.  
619 [https://doi.org/10.1016/S0021-9797\(03\)00149-8](https://doi.org/10.1016/S0021-9797(03)00149-8).
- 620 (92) Shen, J.-W.; Li, C.; van der Vegt, N. F. A.; Peter, C. Understanding the Control of Mineralization by  
621 Polyelectrolyte Additives: Simulation of Preferential Binding to Calcite Surfaces. *J. Phys. Chem. C*  
622 **2013**, *117* (13), 6904–6913. <https://doi.org/10.1021/jp402341w>.
- 623



624

625

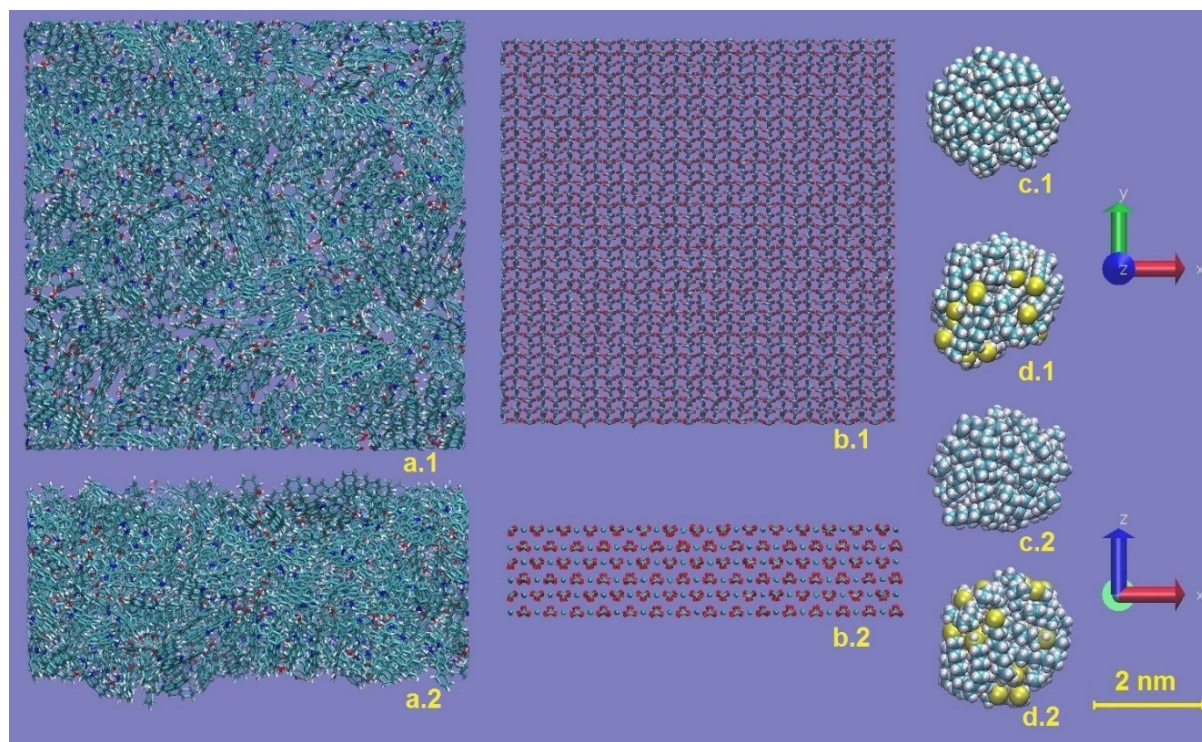
Figure 1. Effect of intermolecular interaction on the fluid confined in nanostructures.



626

627 Figure 2. Molecular structure of type II kerogen fragment (left), non-polar oil n-octane (right top), and  
628 polar oil 1-octanethiol (right bottom).

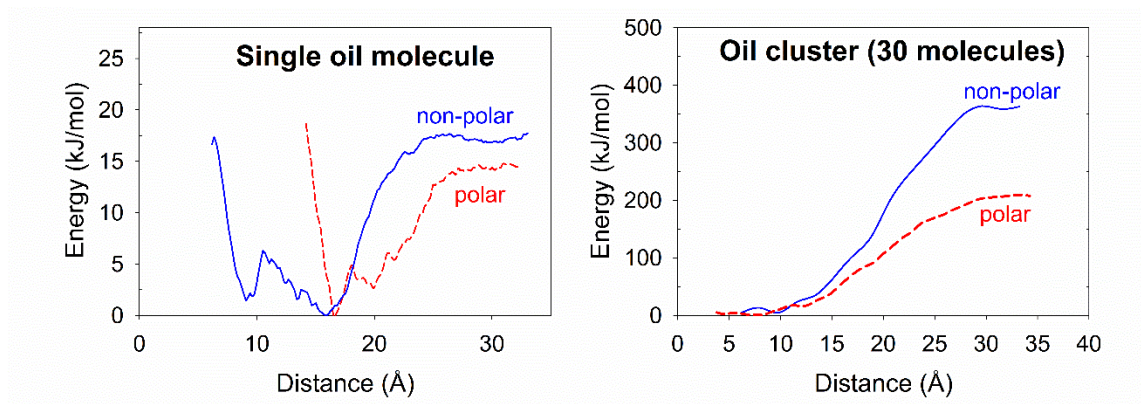
629



630

631 Figure 3. Kerogen slab (a), calcite (104) slab (b), 30-molecule non-polar oil cluster (c), and 30-molecule  
632 polar oil cluster (d). “x.1” and “x.2” denote different orientations.

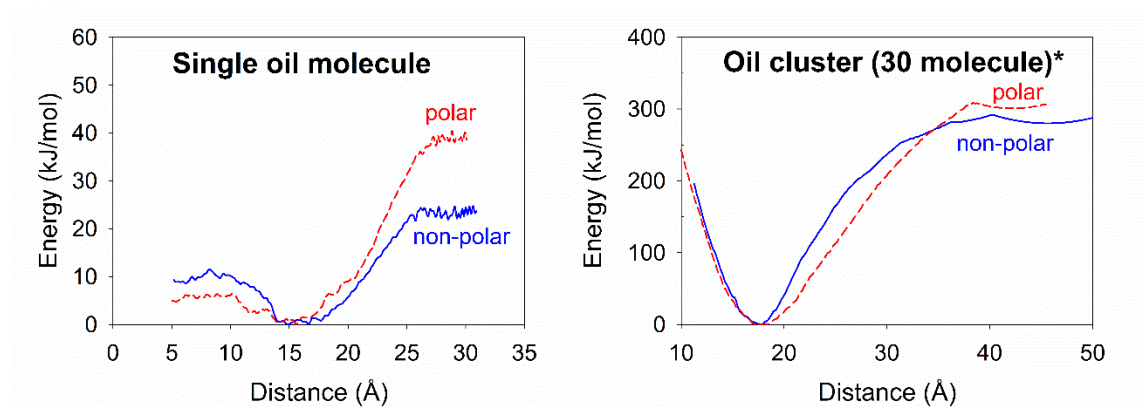
633



634

635 Figure 4. Free energy surfaces of single molecule of polar or non-polar oil on kerogen surface with water  
636 (left); Free energy surfaces of oil drop of 30 polar or non-polar oil molecules on kerogen surface with  
637 water (right).

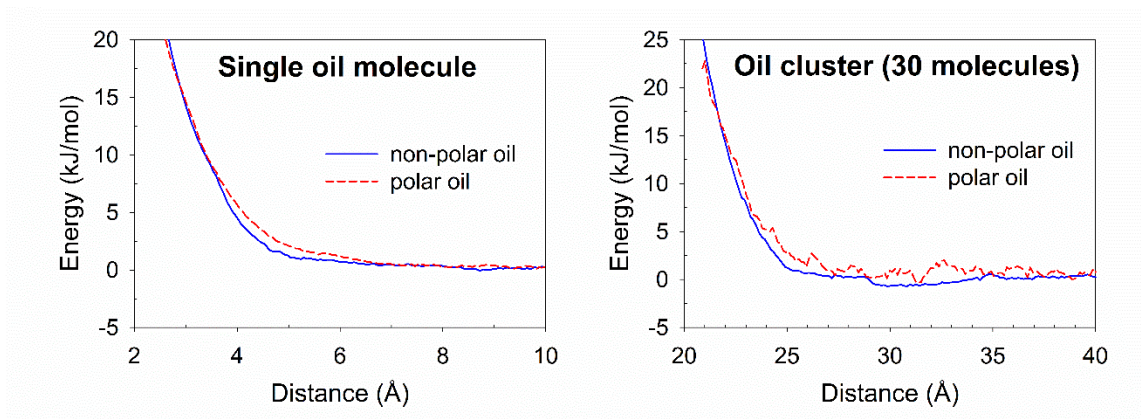
638



639

640 Figure 5. Free energy surfaces of single molecule of polar and non-polar oil on kerogen surface without  
641 water (left); free energy surfaces of oil drop of 30 polar or non-polar oil molecules on kerogen surface  
642 without water (right). \*indicates the simulations were prepared at 200K due to the technical issues as  
643 described in the discussion.

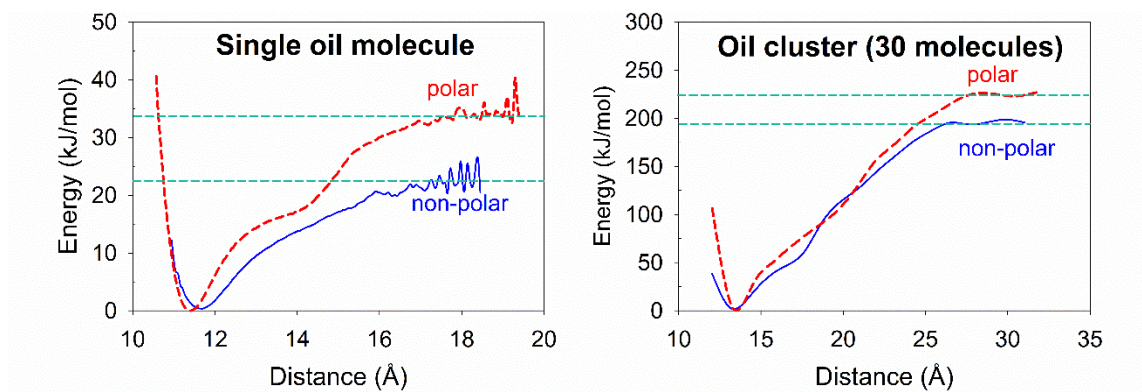
644



645

646 Figure 6. Free energy surfaces of single molecule and 30-molecule cluster of polar or non-polar oil on  
647 calcite surface in the presence of water.

648



649

650 Figure 7. Free energy surfaces of single molecule of polar or non-polar oil on calcite surface without  
651 water (left); free energy surfaces of oil drop of polar or non-polar oil on calcite surface without water  
652 (right).

653



Table 1. Desorption energy of single molecule oil droplet and 30-molecule oil drop on calcite and kerogen surface under 300 K. The ( ) denotes the errors propagated from the output data of WHAM.

Desorption energy (kJ/mol)		Kerogen with water	Kerogen	Calcite with water	Calcite
Non-polar oil	Single molecule	17.0 (2.0)	23.3 (3.5)	0	18.0 (5.5)
	Cluster - total	372 (13.8)	438 (13.5)	0	198 (42)
	Cluster - per molecule	12.4 (0.46)	14.6 (0.45)	0	6.6 (1.4)
Polar oil	Single molecule	16.5 (3.3)	39.5 (9.5)	0	33.6 (3.9)
	Cluster - total	210 (11.4)	438 (13.5)	0	222 (36)
	Cluster - per molecule	7.0 (0.38)	14.6 (0.45)	0	7.4 (1.2)

655 **Supplement Information**

656

657 Code for error estimation performed by RStudio

658

659 library(bootstrap)

660 attach(dat)

661

662 B<-150

663 boot.fit<-matrix(0,B,length(x))

664

665 for (i in 1:B){

666 set.seed(i)

667 indx <- sample(1:178,size=178,replace=T)

668

669 fit <- loess(y~x,dat[indx,],span=0.30)

670

671 boot.fit[i,] <- predict(fit,x)

672 }

673

674 FUN<-function(x){

675 quantile(x,prob=c(.025,.975),na.rm=T) # calculate 95% CI

676 }

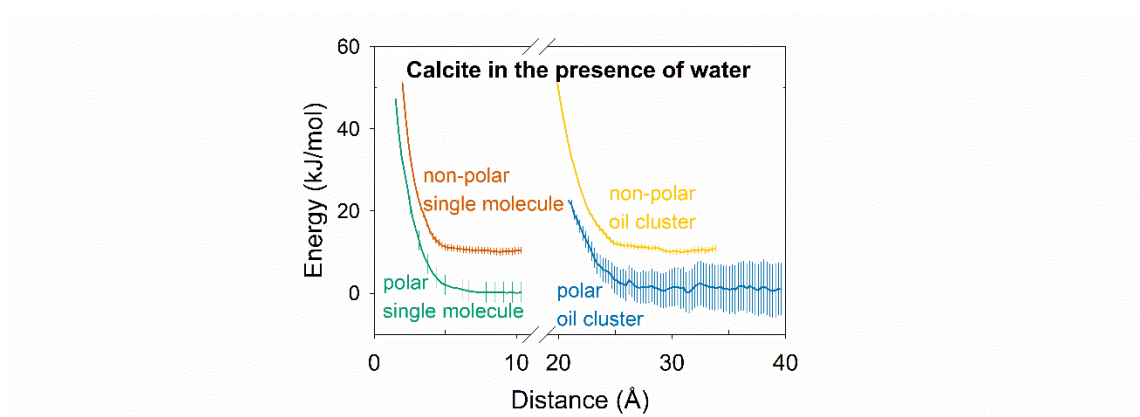
677 boot.CI<-apply(boot.fit,2,FUN)

678

679 y\_2.5<-boot.CI[1,]

680 y\_97.5<-boot.CI[2,]

681

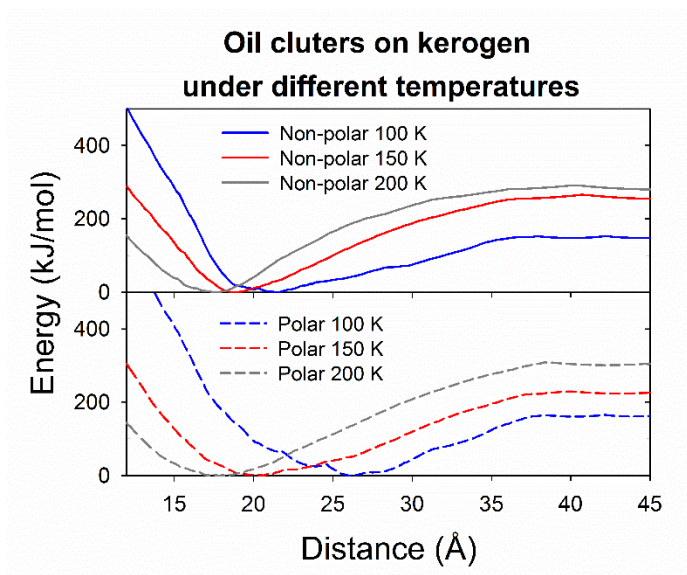


682

683 Figure S1. Free energy surfaces of oil drop of polar or non-polar oil on calcite surface with water. The  
684 density of displayed data is reduced for visual clarity.

685

686

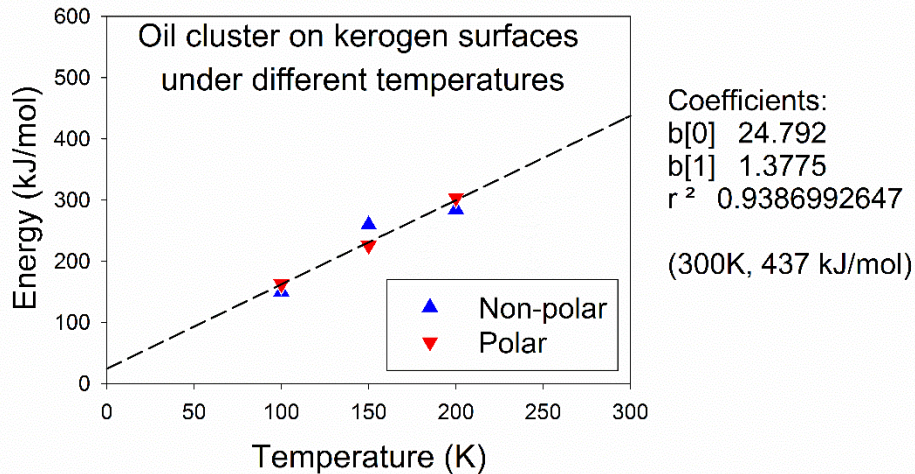


687

688 Figure S2. Free energy surfaces of 30-molecule oil drops interacting with kerogen surface under different  
 689 temperatures. According to the data point pattern on this chart, the correlation between desorption energy  
 690 and temperature can be formulated using the same equation below for both polar and non-polar oil. The  
 691 error bars are smaller than the symbol size.

692

693



694

695 Figure S3. Desorption energies of 30-molecule oil drops on kerogen surfaces under different  
696 temperatures.

697

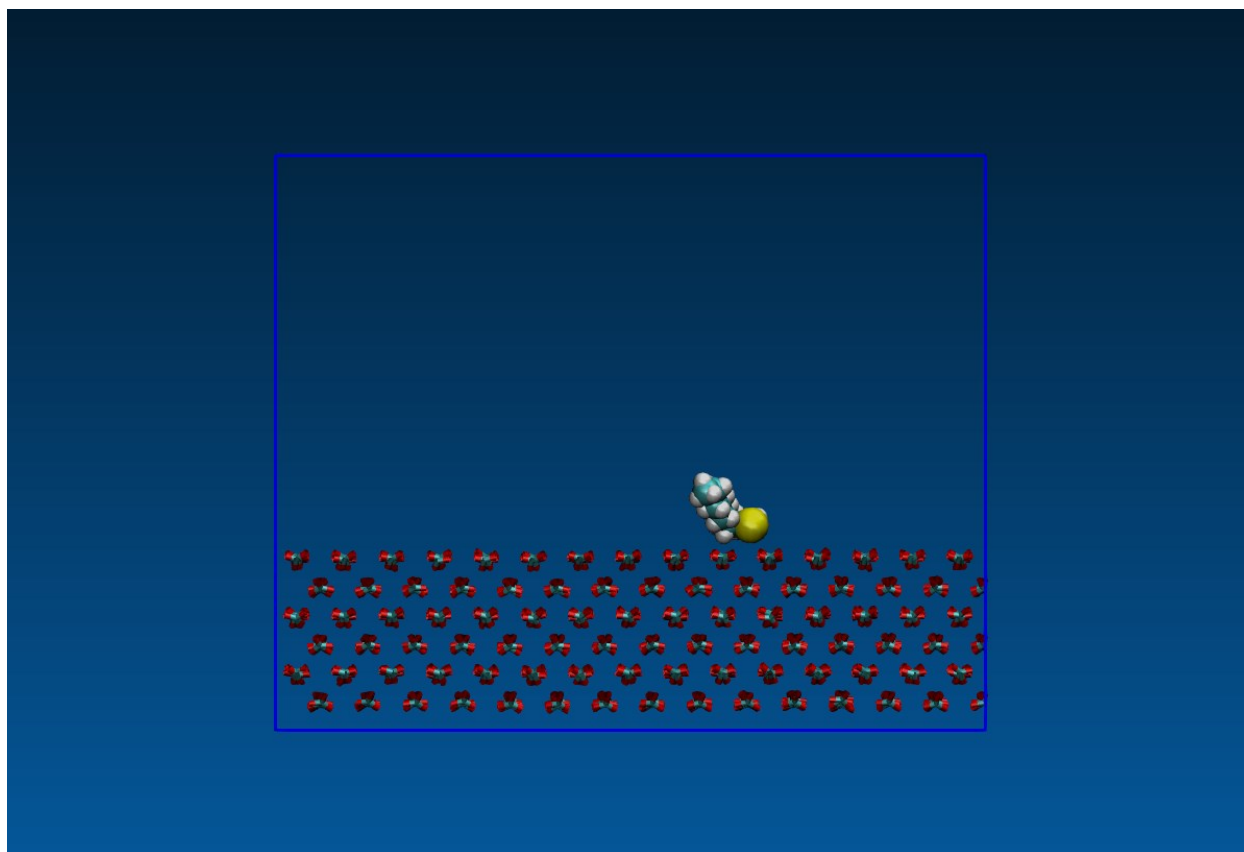
698 The non-polar and polar oil drops exhibit linear relationship between temperature and desorption  
699 energy (with a R-squared value of 0.9387). The non-polar and polar oil drops follow the same  
700 correlation between desorption energy ( $E_d$  in kJ/mol) and temperature ( $T$  in K):

701

$$E_d = 1.38 \cdot T + 24.8$$

702 The energy required for oil drop desorption from kerogen surface increases when the system  
703 temperature rises. As shown in Figure S5, a close examination on the interface of oil and surface  
704 reveals that oil molecule is strongly attached to the kerogen surface. The same correlation of  
705 energy and temperature suggested that the intermolecular bonding between kerogen and oil are  
706 so strong that the effect of oil polarity is negligible in such interactions.

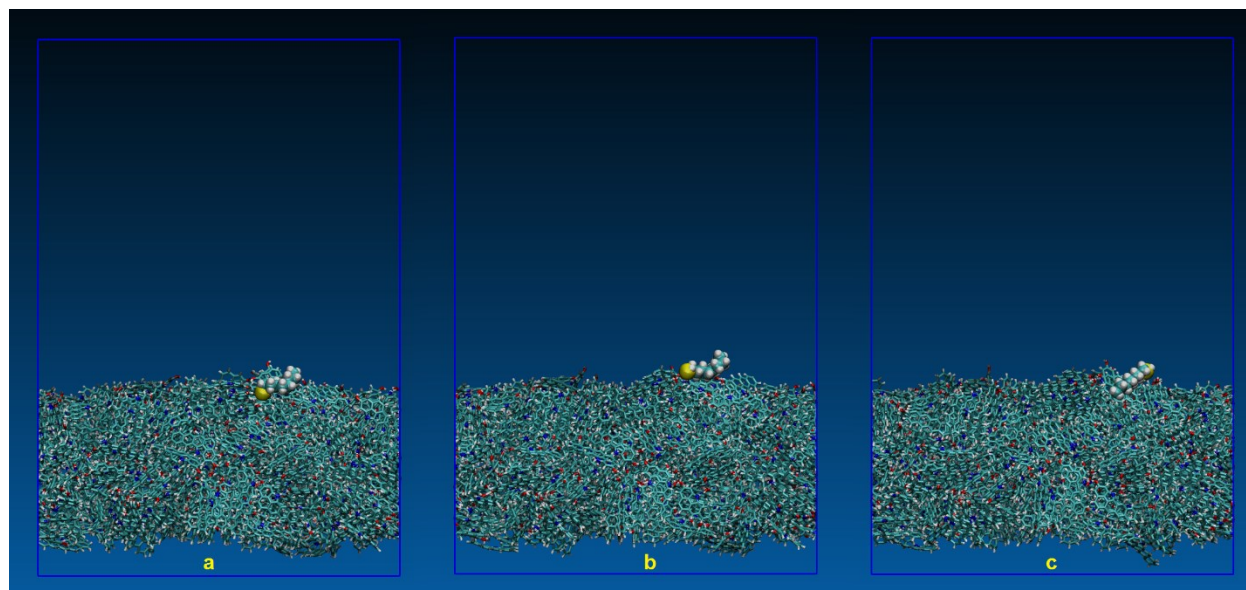
707



708

709 Figure S4. Snapshot of the simulation trajectory of calcite surface interaction with polar oil  
710 molecule in the absence of water.

711



712

713 Figure S5. Snapshot of the simulation trajectory of kerogen surface interaction with polar oil  
714 molecule in the absence of water at different time step. (a) and (b) depict strong interactions  
715 between polar oil functional group  $-SH$  and kerogen functional groups  $-NH-$  and  $-OH$ , whereas  
716 (c) illustrates strong interactions between non-polar carbon chain of polar oil and non-polar  
717 benzene rings of kerogen.

718

719 Table S1. Desorption energies of oil drops on kerogen surface under different temperatures in the absence  
720 of water.

Desorption energy in kJ/mol [error]		
Temperature	Non-polar	Polar
100 K	150.5 [2.5]	163 [3]
150 K	260 [5.5]	226 [3]
200 K	285 [5.5]	304 [5]

721